ChemComm

COMMUNICATION

View Article Online
View Journal | View Issue

Cite this: *Chem. Commun.*, 2024, **60**, 8852

Received 17th May 2024,
Accepted 18th July 2024

DOI: 10.1039/d4cc02402h

rsc.li/chemcomm

Molecular islands at the liquid–solid interface†

Yi Hu, [ab] Kazukuni Tahara *[c] and Steven De Feyter *[a]

Molecular islands of various shapes and sizes composed of a few tens of molecules only are formed at the liquid–solid interface, at room temperature, by an alkoxylated dehydrobenzo[12]annulene (DBA) derivative. Molecules are packed into hexagons. Scanning tunneling microscopy reveals the variety in molecular island structures and their stability. For molecular islands up to 7 hexagonal pores, all 244 possible structures are simulated and compared with experimental observations. Force field calculations give insights into the relative stability of the molecular islands and the factors contributing to it.

Self-assembly of molecules on a solid surface is regarded as a promising method for making defined two- or even three-dimensional (2D, 3D) structures.[1–3] By selecting the solvent and substrate, and controlling the solute concentration and temperature, diverse self-assembled molecular networks (SAMNs) can be constructed.[4–7] Moreover, strategies such as host–guest chemistry, chiral induction and amplification, and confinement effects have been investigated in order to regulate the molecular arrangement in SAMNs.[2,3,8,9] The self-assembled structures are stabilized *via* non-covalent interactions.[10–12] Research of SAMNs has witnessed rapid progress in supramolecular chemistry, nanoscience and technology, and interfacial materials.[13,14] The SAMN formation process at the liquid–solid interface is often described in terms of classical theories involving nucleation, free growth, and ripening, and under favorable dynamic growth conditions, a large area thermodynamically stable phase may be formed.[15]

Scanning tunnelling microscopy (STM) is a preferred tool to visualize the packing of molecules on conductive substrates.[16,17] Few studies address the formation of very small, isolated domains at the liquid–solid interface, in contrast to studies under ultrahigh vacuum conditions.[18–25] Small clusters of molecules at the liquid–solid interface are often very dynamic (in-plane and out-of-plane dynamics) at the time scale of STM imaging and may remain undetected. Often, successful STM imaging goes hand in hand with the formation of SAMNs covering the full surface, consisting of a mosaic of domains with different sizes, shapes, and orientations.[8,9]

In this work, we explored the formation and self-assembly of very small domains which are constructed by several dozens of molecules only. An alkoxylated dehydrobenzo[12]annulene (DBA) derivative, DBA-OC13 (Fig. 1a), was selected, familiar to us from previous studies,[4,16,26] as we noticed the unusual stability of very small clusters, under submonolayer coverage conditions, *i.e.* at low DBA-OC13 concentrations (1.0×10^{-6} M and lower). Under this condition, DBA-OC13 forms molecular clusters or islands with hexagonal pores at the interface between 1-phenyloctane and highly ordered pyrolytic graphite (HOPG) (Fig. 1b–d). STM results reveal that for the same number of hexagonal pores, molecular islands of different structures are formed. According to the experimental data, we simulated all the possible DBA-OC13

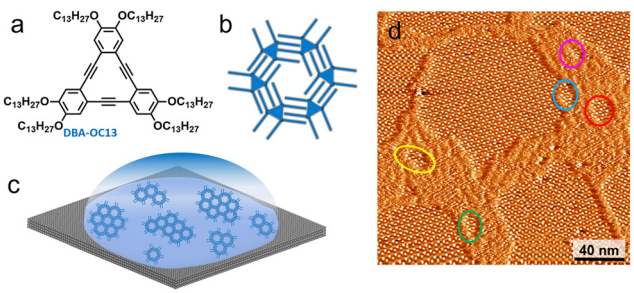

Fig. 1 (a) Chemical structure of DBA-OC13. (b) Schematic model of a hexagonal porous structure. (c) Schematic illustration of the formation of molecular "islands" at the liquid–solid interface. (d) Large-scale STM image of SAMNs formed by DBA-OC13 at the 1-phenyloctane–HOPG interface. Ovals in different colors indicate different small molecular "islands" around the large "islands". Scanning parameters: V_s = −0.20 V, I_t = 200 pA.

[a] *Division of Molecular Imaging and Photonics, Department of Chemistry, KU Leuven, 3001 Leuven, Belgium. E-mail: steven.defeyter@kuleuven.be*
[b] *Institute for Advanced Study, Shenzhen University, Shenzhen 518060, China*
[c] *Department of Applied Chemistry, School of Science and Technology, Meiji University, Kawasaki, Kanagawa 214-8571, Japan. E-mail: tahara@meiji.ac.jp*

† Electronic supplementary information (ESI) available: Experimental details regarding sample preparation, STM imaging, molecular island models and calculation of intermolecular interactions. See DOI: https://doi.org/10.1039/d4cc02402h

clusters as a function of the number of hexagons formed. With Dreiding force field calculations, the intermolecular interactions were determined and are used as one of the elements to assess the stability of the molecular islands.

At a low concentration of 1.0×10^{-6} M, STM observation reveals that all the DBA-OC13 molecules are arranged into a hexagonal porous structure (Fig. 1d and Fig. S1 and S2) at the interface between HOPG and 1-phenyloctane. The experimental details are described in the ESI.† At this concentration, the HOPG surface cannot be entirely covered. Separated domains form, which match the classical view of a nucleation and growth process. An interesting phenomenon is that besides the large domains, some isolated small domains coexist (Fig. 1d), which we refer to as molecular islands. Such small islands are rarely reported at the liquid–solid interface.[26] Their appearance must be the result of stabilizing intermolecular interaction. The islands are typically surrounded by bright fuzzy features, which arise most likely because of mobile DBA or solvent molecules on the surface. We consider that these mobile molecules contribute to the formation of the isolated small islands. Moreover, a concentration-determined moderate growth rate to nucleation rate ratio also contributes to the island formation.

We experimentally identified 15 types of molecular islands (Fig. 2). Their STM images are sorted by increasing number of supramolecular pores. Models for these 15 patterns are summarized in Fig. S3 (ESI†). In addition to the regular hexagonal pores, some pentagonal pores and filled hexagonal pores, the latter being most likely the result of auto host–guest complexation, were observed as well (Fig. 2). We have previously reported that the formation of the pentagonal pores is promoted on defect-rich substrates, while the host–guest pores tend to appear at higher solution concentrations.[4,27,28] Since they represent only a minority in the current study and disappear in time after continuous scanning, these pores were excluded from statistical analysis and force field calculations (*vide infra*).

Moreover, some isolated molecules at the edge of the hexagonal pores are also not stable. Successive STM scanning of the same area revealed their dynamic appearance and disappearance (Fig. S4, ESI†). From these results, we conclude that for stable STM imaging at the liquid–solid interface, the DBA-OC13 molecules should be involved in a hexagonal pore framework.

For the same number of hexagonal pores, DBA-OC13 molecules can pack into molecular islands of different shapes (Fig. 2). For example, for the case of five pores, two different islands are observed (Fig. 2e_1 and e_2). We define the number of hexagonal pores as n. The larger the value of n, the more different island patterns may theoretically form. Nevertheless, the experimentally observed number of patterns for a given value of n ($n > 3$) is far below what is theoretically possible. Hence, the question arises: what limits the number of experimentally observed molecular island patterns?

Force field calculations were carried out to compare the intermolecular interaction energies of the observed molecular islands. The details on the force field calculation, the optimized island models (Fig. S3), and the calculated energies (Table S1) are described in the ESI.† Molecule–substrate interaction energies were ignored, as we did not expect them, at the level of individual molecules, to depend on the island size. Anyhow, we ran some tests and fluctuations in the molecule–substrate interaction energy value were indeed not island size related. Let us take the three-pore shapes in Fig. 2c_1 and c_2 as examples for the consideration of the intermolecular interaction energies.

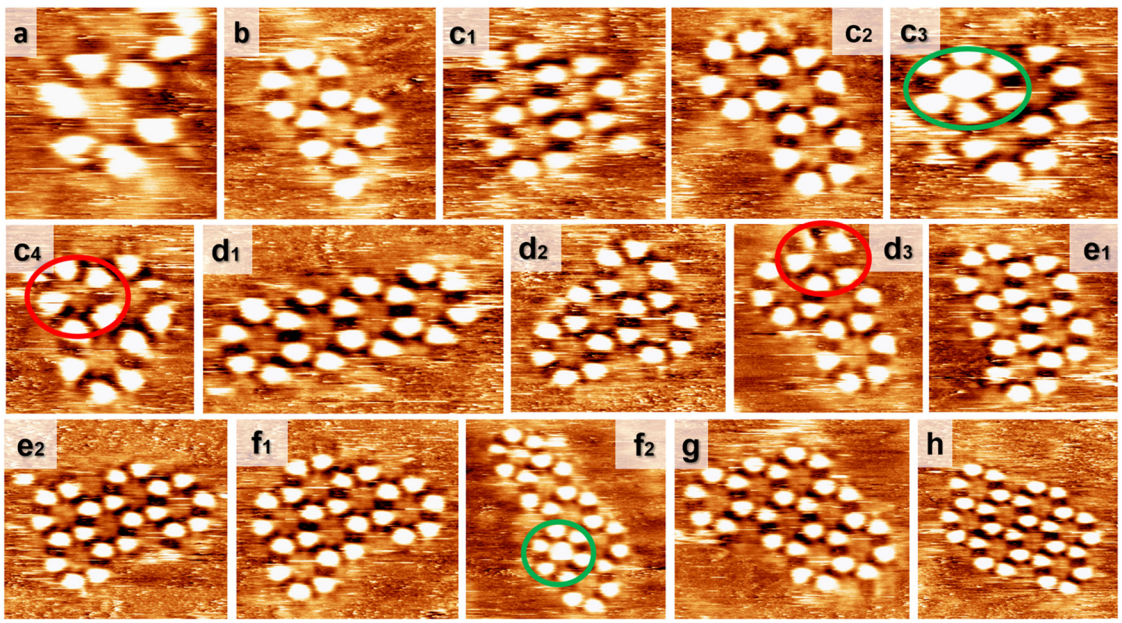

Fig. 2 STM images of different kinds of molecular islands that contain (a) 1 pore, (b) 2 pores, (c_1)–(c_4) 3 pores, (d_1)–(d_3) 4 pores, (e_1) and (e_2) 5 pores, (f_1) and (f_2) 6 pores, (g) 7 pores and (h) 8 pores. The green and red ovals indicate the host–guest and pentagonal pores, respectively. Scanning parameters: V_s = −0.20 V, I_t = 200 pA.

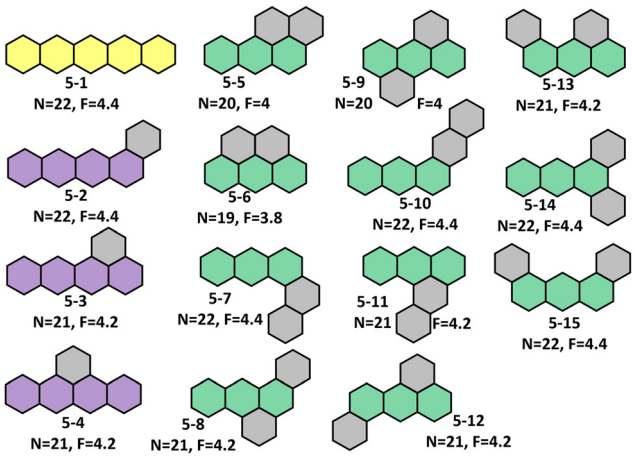

Fig. 3 Schematic diagrams of the 15 possible models for n = 5. N represents the total number of DBA-OC13 molecules in every model. 5-1 to 5-15 are their serial numbers. The longest linear strand of adjacent hexagonal pores is indicated in color.

Their intermolecular interactions were calculated to be −97.6 and −96.0 kJ mol^{-1} per molecule, respectively. Note though that energy must be compared taking the difference in the number of molecules into account. Therefore, a parameter (F) that reflects the relationship between the number of hexagonal pores (n) and DBA-OC13 molecules (N) is introduced.

$$F(n, N) = N/n$$

The value of $F(n, N)$ denotes the average number of DBA-OC13 molecules per hexagonal pore.

We simulated all possible models with n changing from 1 to 7 (Fig. S6, ESI†). This resulted in 244 models. Their schematic diagrams are summarized in the ESI.† As an example, the 15 possible models for n = 5 are shown in Fig. 3, which are numbered from 5-1 to 5-15. The number of DBA-OC13 molecules ranges from N = 19 to N = 22. The more common edges these hexagonal pores have, the lower the value of N is. More common edges result in more compact islands. Therefore, F is a measure of the compactness of the molecular islands. The lower the value of F, the more compact the islands, and *vice versa*.

Fig. 4 shows the relationship between the intermolecular interaction energies of these 244 simulated models and F, expressed per hexagonal pore and per molecule. As F increases, the total intermolecular interaction energy per pore increases (Fig. 4a), which is the logical consequence of the increasing average number of DBA-OC13 molecules per hexagonal pore.

It is clear that the smaller the F, the larger the intermolecular interaction energy per molecule (Fig. 4b), as the number of interactions per molecule increases. Consider the two models numbered 5-1 and 5-6 in Fig. 3. 5-1 (F = 4.4) is a linearly arranged structure, while 5-6 (F = 3.8) is a compact island. Their intermolecular interactions are −100.6 and −103.3 kJ mol^{-1} per molecule, indicating larger intermolecular interaction energies for compact islands. Moreover, according to our STM data, as the hexagonal pore number increases, *e.g.* $n \geq 5$, the linearly arranged islands with the largest F value have never been observed. In summary, at the level of intermolecular interaction energies, a more compact packing of DBA-OC13 (low F value) is preferred over a less compact one (high F value).

Does this also mean that islands with a low aspect ratio are thermodynamically more stable than those with a high aspect ratio? First of all, it is important to note that kinetic effects[29,30] are ignored, which may be justified given that the islands remain dynamic even after the islands are formed (Fig. S4, ESI†). A rigorous quantitative approach to assess the thermodynamics, which would involve diverse experimental methodologies, is beyond the scope of this study and is not possible given that the islands are minority species on the substrate.[31] Qualitatively speaking, the enthalpy gain due to van der Waals interactions between interdigitated alkyl chains comes at an entropy cost (translational, rotational, conformational). One may argue that the entropy cost due to alkyl chain interdigitation will be larger than the entropy cost for alkyl chains at the rim of molecular islands, as these alkyl chains may be partly desorbed. Following this reasoning, from an entropy point of view, islands with a large aspect ratio and a large rim with few interdigitated alkyl pairs should actually be more stable. Experiments show the

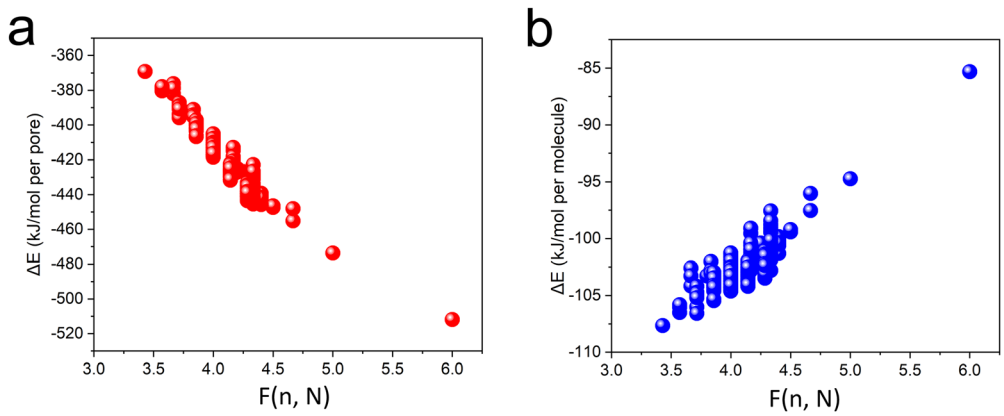

Fig. 4 Calculation of the intermolecular interaction energies for the 244 molecular islands corresponding to $n < 8$, expressed (a) per hexagonal pore and (b) per molecule. Many data points overlap. The molecular islands that correspond to those in Fig. 2 are highlighted in Fig. S5 (ESI†).

opposite. Therefore, while simplified, the interaction energy per molecule or pore is considered a good proxy for the experimentally observed island stability, at least in this study.

In conclusion, we successfully identified small molecular islands at the liquid–solid interface. These islands are formed by an alkoxylated dehydrobenzo[12]annulene derivative, DBA-OC13. These separated clusters are stable on HOPG. Based on the STM observation of such molecular islands, force field calculations were conducted. For the representation of a given molecular island shape, we introduced the function $F(n, N)$ which is the average number of DBA-OC13 molecules per pore. Therefore, F is a measure of the structural compactness. The force field calculations for 244 possible molecular island models with n = 1–7 suggest that the lower the F value, the more stable the molecular island will be, taking into account some enthalpy and entropy considerations. When forming a molecular island, DBA-OC13 molecules prefer to arrange in a more compact shape (low aspect ratio), which can be explained on the basis of intermolecular interaction energies.

This work was supported by Shenzhen Science and Technology Program (RCBS20210609103228020). S. D. F. thanks KU Leuven – Internal Funds (C14/23/090) for financial support. K. T. acknowledges the support by JSPS KAKENHI Grant Number JP20H02553.

Data availability

The data supporting this article have been included as part of the ESI.†

Conflicts of interest

There are no conflicts to declare.

Notes and references

1 H. Zou, L. Liu, S. Zhang, X. Miao, L. Ying, W. L. Deng and Y. Cao, *J. Phys. Chem. Lett.*, 2023, **14**, 489–498.
2 S. Zhang, L. Cheng, C. Chen, J. Li, X. Li, M. Zhang, F. Cheng, X. Xiao, K. Deng and Q. D. Zeng, *Langmuir*, 2021, **37**, 2153–2160.
3 S. Lu, D. J. Morrow, Z. Li, C. Guo, X. Yu, H. Wang, J. D. Schultz, J. P. O'Connor, N. Jin, F. Fang, W. Wang, R. Cui, O. Chen, C. Su, M. R. Wasielewski, X. Ma and X. Li, *J. Am. Chem. Soc.*, 2023, **145**, 5191–5202.
4 Y. Hu, A. M. Bragança, L. Verstraete, O. Ivasenko, B. E. Hirsch, K. Tahara, Y. Tobe and S. De Feyter, *Chem. Commun.*, 2019, **55**, 2226–2229.
5 B. Zha, X. Miao, P. Liu, Y. Wu and W. L. Deng, *Chem. Commun.*, 2014, **50**, 9003–9006.
6 A. Mahmood, X. Zeng, A. S. Saleemi, K.-Y. Cheng and S.-L. Lee, *Chem. Commun.*, 2020, **56**, 8790–8793.
7 T. Chen, S. Y. Li, D. Wang, M. Yao and L. J. Wan, *Angew. Chem., Int. Ed.*, 2015, **54**, 4309–4314.
8 Y. Fang, E. Ghijsens, O. Ivasenko, H. Cao, A. Noguchi, K. S. Mali, K. Tahara, Y. Tobe and S. De Feyter, *Nat. Chem.*, 2016, **8**, 711–717.
9 J. Seibel, L. Verstraete, B. E. Hirsch, A. M. Bragança and S. De Feyter, *J. Am. Chem. Soc.*, 2018, **140**, 11565–11568.
10 F. Cheng, X.-J. Wu, Z. Hu, X. Lu, Z. Ding, Y. Shao, H. Xu, W. Ji, J. Wu and K. P. Loh, *Nat. Commun.*, 2018, **9**, 4871.
11 X.-Y. Wang, T.-F. Jiao, Z.-X. Zhang, T. Chen, M.-H. Liu, L.-J. Wan and D. Wang, *J. Phys. Chem. C*, 2013, **117**, 16392–16396.
12 P. Henkel, K. L. H. Pohl and D. Mollenhauer, *J. Phys. Chem. C*, 2024, **128**, 5848–5859.
13 I. C.-Y. Hou, V. Diez-Cabanes, A. Galanti, M. Valášek, M. Mayor, J. Cornil, A. Narita, P. Samorì and K. Müllen, *Chem. Mater.*, 2019, **31**, 6979–6985.
14 A. G. Slater, L. M. A. Perdigão, P. H. Beton and N. R. Champness, *Acc. Chem. Res.*, 2014, **47**, 3417–3427.
15 K. Kim, K. E. Plass and A. J. Matzger, *Langmuir*, 2003, **19**, 7149–7152.
16 Y. Fang, K. Tahara, O. Ivasenko, Y. Tobe and S. De Feyter, *J. Phys. Chem. C*, 2018, **122**, 8228–8235.
17 G. Binnig and H. Rohrer, *Surf. Sci.*, 1983, **126**, 236–244.
18 M. Böhringer, K. Morgenstern, W.-D. Schneider, R. Berndt, F. Mauri, A. De Vita and R. Car, *Phys. Rev. Lett.*, 1999, **83**, 324–327.
19 T. Yokoyama, S. Yokoyama, T. Kamikado, Y. Okuno and S. Mashiko, *Nature*, 2001, **413**, 619–621.
20 J. Shi, Y. Li, X. Jiang, H. Yu, J. Li, H. Zhang, D. J. Trainer, S. W. Hla, H. Wang, M. Wang and X. Li, *J. Am. Chem. Soc.*, 2021, **143**, 1224–1234.
21 H. Kong, L. Wang and W. Xu, *J. Phys. Chem. C*, 2021, **125**, 354–357.
22 G. Eder, E. F. Smith, I. Cebula, W. M. Heckl, P. H. Beton and M. Lackinger, *ACS Nano*, 2013, **7**, 3014–3021.
23 R. Zuzak, O. Stoica, R. Blieck, A. M. Echavarren and S. Godlewski, *ACS Nano*, 2021, **15**, 1548–1554.
24 J. P. D. C. Calupitan, O. Guillermet, O. Galangau, M. Yengui, J. Echeverría, X. Bouju, T. Nakashima, G. Rapenne, R. Coratger and T. Kawai, *J. Phys. Chem. C*, 2018, **122**, 5978–5991.
25 Z. Huang, Y. Lin, C. Han, Y.-Y. Sun, K. Wu and W. Chen, *J. Phys. Chem. C*, 2021, **125**, 7944–7949.
26 Y. Sato, S. De Feyter and K. Tahara, *Langmuir*, 2023, **39**, 16825–16832.
27 A. M. Braganca, B. E. Hirsch, A. Sanz-Matias, Y. Hu, P. Walke, K. Tahara, J. N. Harvey, Y. Tobe and S. De Feyter, *J. Phys. Chem. C*, 2018, **122**, 24046–24054.
28 H. Cao, I. Destoop, K. Tahara, Y. Tobe, K. S. Mali and S. De Feyter, *J. Phys. Chem. C*, 2016, **120**, 17444–17453.
29 K. Gurdumov, U. Mazur and K. W. Hipps, *J. Phys. Chem. C*, 2022, **126**, 12916–12927.
30 K. W. Hipps and U. Mazur, *Langmuir*, 2018, **34**, 3–17.
31 W. Song, N. Martsinovich, W. M. Heckl and M. Lackinger, *J. Am. Chem. Soc.*, 2013, **135**, 14854–14862.